








MSAB limits osteoarthritis development and progression through inhibition of β -catenin-DDR2 signaling

Ke Lu^{a,b,c,1} , Zhidong Liao^{a,b,1} , Jingwen Li^{a,d,1}, Yuhan Wang^e,
Yuting Zhang^a , Lintao Cai^f, William W. Lu^b , Fan Yang^a, Hong Pan^{e,f,**}, Di Chen^{a,b,*} 

^a Research Center for Computer-aided Drug Discovery, Shenzhen Institute of Advanced Technology, Chinese Academy of Sciences, Shenzhen, 518055, China

^b Faculty of Pharmaceutical Sciences, Shenzhen University of Advanced Technology, Shenzhen, 518055, China

^c Shenzhen Hospital, Southern Medical University, Shenzhen, 518000, China

^d Department of Biomedical Engineering, Southern University of Science and Technology, Shenzhen, 518055, China

^e Guangdong Key Laboratory of Nanomedicine, CAS-HK Joint Lab of Biomaterials, CAS Key Laboratory of Biomedical Imaging Science and System, Shenzhen Institute of Advanced Technology, Chinese Academy of Sciences, Shenzhen, 518055, China

^f Sino-Euro Center of Biomedicine and Health, Luohu, Shenzhen, 518024, China

ARTICLE INFO

Keywords:

Osteoarthritis

MSAB

β -catenin

DDR2

Cartilage degeneration

OA pain

ABSTRACT

The aberrant activation of the canonical Wnt/ β -catenin signaling has been identified as a significant contributor to the pathogenesis of osteoarthritis (OA), exacerbating OA symptoms and driving OA progression. Despite its potential as a therapeutic target, clinical translation is impeded by the lack of a targeting delivery system and effective drug candidate that can modulate steady-state protein levels of β -catenin at post-translational level. Our study addresses these challenges by offering a new approach for OA treatment. To overcome these challenges, we introduced a novel delivery system using human serum albumin (HSA) to deliver a small molecule β -catenin inhibitor, Methyl-Sulfonyl AB (MSAB). This system is designed to enhance the bioavailability of MSAB, ensuring its accumulation inside the joint space, and facilitating the degradation of β -catenin protein. We have demonstrated that MSAB, when delivered via HSA, not only effectively inhibits cartilage damage but also ameliorates OA-related pain in an OA mouse model. We then performed proteomic analysis and biochemical studies to determine the molecular mechanisms underlying the therapeutic effects of MSAB. We identified that discoidin domain receptor 2 (DDR2), a critical mediator in OA pathology, is a downstream molecule of β -catenin signaling and β -catenin/TCF7 directly controls DDR2 gene transcription. MSAB suppressed the DDR2 expression in chondrocytes. MSAB ameliorated OA progression and OA-associated pain through inhibition of β -catenin-DDR2 signaling. This study underscores the efficacy of MSAB/HSA in OA treatment, providing new insights into its molecular mechanism of OA. It suggests that targeted therapies with MSAB/HSA could be a new OA management strategy.

1. Introduction

Osteoarthritis (OA), also known as degenerative joint disease characterized by the progressive degradation of joint cartilage [1]. It affects a significant global population, particularly the elderly, and is influenced by multiple factors, such as aging, obesity, genetic predisposition, and joint injuries. The pathogenesis of this disease involves an imbalance

between cartilage degradation and anabolic regeneration, resulting in pain, stiffness, and impaired joint mobility. Current therapeutic strategies primarily aim at managing symptoms and enhancing joint functionality through non-pharmacological interventions, analgesics, and surgical interventions [2]. However, the challenges of discovering a cure, addressing long-term pain medication usage, and ensuring equitable access to healthcare persist. Further investigation is warranted to

* Corresponding author. Research Center for Computer-aided Drug Discovery, Shenzhen Institute of Advanced Technology, Chinese Academy of Sciences, Shenzhen, 518055, China.

** Corresponding author. Guangdong Key Laboratory of Nanomedicine, CAS-HK Joint Lab of Biomaterials, CAS Key Laboratory of Biomedical Imaging Science and System, Shenzhen Institute of Advanced Technology, Chinese Academy of Sciences, Shenzhen, 518055, China.

E-mail addresses: hong.pan@siat.ac.cn (H. Pan), di.chen@siat.ac.cn (D. Chen).

¹ These authors contributed equally to this work.

<https://doi.org/10.1016/j.bioactmat.2024.10.023>

Received 12 March 2024; Received in revised form 12 October 2024; Accepted 22 October 2024

Available online 24 December 2024

2452-199X/© 2024 The Authors. Published by KeAi Communications Co., Ltd. This is an open access article under the CC BY-NC-ND license (<http://creativecommons.org/licenses/by-nc-nd/4.0/>).

elucidate the molecular mechanisms underlying OA and develop more efficacious treatment modalities [3].

The aberrant activation of the Wnt/ β -catenin signaling pathway plays a pivotal role in the pathogenesis of OA in various joints, including the knee, hip, mandibular, and facet joints [4–7]. Activation of the β -catenin signaling pathway leads to degradation of the cartilage matrix, induction of chondrocyte hypertrophy and apoptosis, and exacerbation of chronic pain in OA through upregulation of inflammatory factors such as CCL2 [5,7]. Therefore, the identification of an effective inhibitor of β -catenin is of utmost importance for OA treatment [8,9]. Methyl-Sulfonyl AB (MSAB) is a potent and selective inhibitor of Wnt/ β -catenin signaling that has demonstrated significant anti-tumor effects in Wnt-dependent cancer cells. In mouse xenograft models, MSAB has been shown to reduce the size and weight of various types of Wnt-dependent tumors, including HCT116, HT115, and H23 [10]. However, the precise role of MSAB in the context of OA is currently unknown.

The selection of an appropriate drug delivery system for the treatment of OA is of utmost importance in ensuring sustained and controlled release of drugs, targeted delivery to the affected joint or tissue, effective management of symptoms, and enhanced patient compliance [11–13]. Therefore, we have opted for the utilization of human serum albumin (HSA) nanoparticles as a drug delivery system to deliver MSAB. HSA nanoparticles have emerged as a highly promising drug delivery system owing to their remarkable biocompatibility, high drug-loading capacity, stability, prolonged circulation time, targeted delivery capabilities, and ease of production [14]. Being a naturally occurring protein, HSA nanoparticles are considered safe and well-tolerated in the body [15]. They possess the ability to efficiently encapsulate a wide range of drugs, including both hydrophobic and hydrophilic compounds, and exhibit prolonged circulation within the bloodstream. Through surface modifications, HSA nanoparticles can be directed towards specific tissues or cells, thereby minimizing off-target effects, and enhancing the therapeutic efficacy [14]. Moreover, their simple and scalable production methods render them cost-effective and suitable for large-scale manufacturing. In conclusion, HSA nanoparticles hold tremendous potential as an effective and versatile drug delivery system.

In this study, we assessed the efficacy of MSAB administered via HSA intra-articular injection in the management of OA using an experimental OA mouse model. Additionally, we investigated the molecular mechanism underlying the alleviation of cartilage destruction and chronic pain in OA by MSAB. Our results revealed that MSAB exhibited protective effects against OA pain through the inhibition of CCL2 expression. Moreover, it effectively mitigated OA cartilage degradation by suppressing the expression of discoidin domain receptor 2 (DDR2).

2. Materials and methods

2.1. Cells and cell culture

ATDC5 cells (Riken Cell Bank, Japan) were cultured according to the vendor's instruction. BIO (1 μ M, 24h) was used to drive ATDC5 cell differentiation, and chondrogenesis markers (*Mmp13*, *Col-X*) were validated by qPCR (Fig. S1). Insulin, transferrin, and selenate (ITS) were used to induce chondrogenesis. Primary chondrocytes were isolated from the knee joint of 10-day-old C57BL/6 mice, and the 2nd passage cells (P2) were used for subsequent experiments. For primary dorsal root ganglion (DRG) cells isolation and culture, the DRGs were rapidly isolated from the nerve-innervated DRGs of 3–4 mice by digestion with 1 mg/mL collagenase IV and 30 U/mL papain (Worthington Biochemical). The isolated DRG cells were then seeded on glass cover slips coated with poly-L-lysine and laminin (20 μ g/mL). ATDC5 cells, primary chondrocytes and primary DRG cells were cultured in DMEM/F12 supplemented with 10 % FBS and penicillin (100 U/ml). All the cells were incubated at 37 °C and 5 % CO₂ in a humidified incubator.

2.2. Protein extraction and Western blot analysis

For Western blot (WB) analysis, cells were washed three times with cold Phosphate Buffered Saline (PBS), and then the lysis buffer (50 mM Tris HCl [pH 7.4], 150 mM NaCl, 20 mM EDTA, 1 % Triton X-100, 1 % sodium deoxycholate, 0.1 % SDS, and protease inhibitors) were added to the cells. The cell lysates were incubated on ice for 30 min, and then the supernatant was taken by centrifugation at 12,000 rpm at 4 °C for 10 min. Protein concentrations were estimated with the protein assay kit and separated by SDS-PAGE using 10 % acrylamide gradients and electro-transferred onto fit PVDF membranes (Bio-Rad, Hercules, California, USA), which were then blocked with PBS buffer containing 5 % non-fat dry milk and 0.1 % Tween-20. The membranes were probed with primary antibodies at 4 °C with gentle shaking overnight. Then membranes were washed and incubated with corresponding secondary antibodies (1:1000) for 1 h at room temperature. After washing in PBST for 30 min, the chemiluminescent signals on the membranes were detected using the ECL reagent (Thermo, USA). The antibodies used in this study were listed in Table S1.

2.3. Immunofluorescence

Cells spread on culture slides were washed twice with cold PBS and fixed with 4 % paraformaldehyde solution for 20 min on ice, then washed twice with PBST. For paraffin sections, sections were sequentially treated with rehydration, antigen retrieval, and Endogenous Peroxidase Blocking Buffer (Beyotime, China) and then treated with 0.5 % Triton X-100 for 10 min. Next, the sections were incubated with the goat serum blocking solution at 37 °C for 30 min. After removing the excess blocking solution, samples were incubated with primary antibodies overnight at 4 °C in a humid environment. After washing three times with PBST, the cells were incubated with the corresponding secondary antibodies for 1h at room temperature. Finally, slides were stained with Antifade Mounting Medium with DAPI (Vector Laboratories, USA) and images were captured using Leica Application Suite X Software on Leica microscope (DM2000 LED, Germany) and analyzed by Image J software (National Institutes of Health, MD, USA). The antibodies used in this study were listed in Table S1.

2.4. RNA extraction and quantitative real-time PCR

Total RNA was extracted from ATDC5 cells treated with or without 20 ng/mL TNF- α and with or without 50 μ M MSAB (Selleck, China) for 24 h using TRIzol reagent (Invitrogen, USA). It was then reverse transcribed by an RT reagent kit (Takara, Japan) for cDNA synthesis. cDNA was amplified by qRT-PCR using primers for *Ddr2*, *Runx2*, *Axin2*, *Ccl2*, *Dkk1*, *Ccnd1*, *Mmp3*, *Mmp13*, *Adamts4*, *Adamts5*, and *Col-X*, which are shown in Table S2. PCR reactions for each sample were performed in triplicate by using the Applied Biosystems by Thermo Fisher Scientific. A comparative Ct ($2^{-\Delta\Delta C_T}$) method was used for analysis, and β -Actin served as internal reference genes.

2.5. Fabrication and characterization of MSAB/HSA nanoparticles

The MSAB/HSA nanoparticle (NP) were developed via ultrasonication method. Briefly, 20 mg of HSA (Sigma-Aldrich, USA) was dissolved in 5 mL double-distilled water (ddH₂O). 200 μ L of chloroform and 50 μ L of anhydrous ethanol were prepared into mixed solvent, then 20 μ L of MSAB (50 mg/mL, RD Systems, USA) was dissolved in chloroform/anhydrous ethanol mixture. The MSAB solution was dripped slowly into HSA solution, and ultrasonicated for 5 min at pH 7.5–8.0 to form MSAB/HSA nanoparticles. The percentage of unpacked MSAB was isolated from fresh HSA nanoparticles via ultrafiltration tube and analyzed by high performance liquid chromatography (HPLC) to assess the encapsulation efficiency of MSAB in nanoparticles. Next, the size distribution and Zeta potential of MSAB/HSA nanoparticle were

determined by a light scattering (DLS) analysis using Zetasizer Nano ZS (Malvern, UK). The morphology of MSAB/HSA nanoparticle was characterized by TEM (FEI TecnaiG2 F20 S-Twin, USA). Finally, the kinetics of MSAB release from HSA nanoparticles were analyzed by HPLC to determine the percentage of released MSAB from 0 h to 72 h.

2.6. *In vivo* imaging analysis

In vivo imaging analysis was performed as described previously [16]. Briefly, ICG-labeled HSA -NP were injected intra-articular into 10-week-old C57BL/6 mice. The mice were anesthetized for *ex vivo* fluorescence imaging using an *in vivo* imaging system (IVIS Spectrum, PerkinElmer, CA) after 5 min, 24h, 48h, and 72h.

2.7. Animal study

Ten-week-old male C57BL/6 mice, weights ranging from 25 g to 30 g (provided by were purchased from GemPharmatech Biotechnology Co., Ltd.) were used in this study. These mice are housed in specific pathogen-free (SPF) animal care facilities at a temperature (22–25 °C), 12-h/12-h day-night cycle, and animals are free to draw water and food in cages. Before the experiment, the mice were left undisturbed for one week to acclimate to the new environment. For the toxicity test of MSAB/HSA, mice were randomly divided into two groups ($n = 7$ in each group) including Vehicle injection group and MSAB/HSA injection group. PBS was used in Vehicle injection group. After 4 weeks injection (twice a week, 1 mg/mL, 20 μ L per intra-articular injection), mice behaviors were assessed by the Laboratory Animal Behavior Observation Registration and Analysis System (LABORASTM, Metris, Netherlands) and tissues including liver, kidney, heart, spleen, knee joint were harvested for histological analysis. For OA treatment study, mice were randomly allocated into three groups ($n = 10$ in each group), including the Ctrl group (Sham operation, vehicle injection), destabilization of the medial meniscus (DMM) surgery with intra-articular injection of vehicle, DMM surgery with intra-articular injection of MSAB/HSA twice a week. The mice knee OA was induced by DMM surgery as previously described [16,17]. In brief, under general anesthesia in mice, DMM surgery was performed by sectioning the medial meniscotibial ligament anchoring medial meniscus to tibial plateau. The control group underwent Sham surgery in which a similar incision was made into the joint capsule and then closed. Schematic diagram depicting the time of treatment and the follow up period of the mice was showed in Fig. S2. The animal protocol of this study has been approved by the Ethics Committee of the Shenzhen Institute of Advanced Technology, Chinese Academy of Sciences and all experimental methods and procedures were carried out in accordance with the approved guidelines (SIAT-IACUC-20230403-YYJ-JSYWZX-LK-A2190-01).

2.8. Pain-related behavior tests

The assessment of spontaneous behavior was measured by LABORASTM, according to protocols as previously described [18]. In brief, after weighing the animals, mice were placed on 4 platforms for testing with unrestricted access to water and food. The test lasted for 12 h from 20:00 p.m. on the first day to 8:00 a.m. on the next day. The parameters analyzed include motion track, the distance of locomotion, average speed of locomotion, climbing and rearing.

OA pain, including mechanical allodynia and thermal allodynia, was assessed by the von Frey filament test and hotplate test as previously described [16,19]. Von Frey test was performed using a calibrated set of von Frey filaments (North Coast Medical Inc., CA, USA). Mice were placed in Plexiglas boxes with mesh flooring and allowed to acclimatize for at least 30 min before assessment. Filaments with loadings ranging from 0.04 g to 6.0 g were used in this experiment. First, 0.4 g of silk was used to apply stimulation to the mid-plantar surface of the hind paw and the 50 % force withdrawal threshold was calculated using the

"up-and-down" method as previously described [16]. Observers performed the test in a blinded fashion.

Thermal nociceptive sensitivity of mice in different experimental groups were evaluated by the hotplate test. In brief, mice were placed in a hotplate platform at room temperature for half an hour to acclimate to the environment and then removed after no longer looking around and exploring, and then placed on the hotplate platform at a temperature of 50 °C (Jiangsu Cyonse Biotechnology Co., LTD., China). The temperature stimulated the hind limbs of the mice to produce a painful response, such as shaking, jumping, or licking, and reaction times were recorded. Observers performed the test in a blinded fashion.

2.9. Histological analysis

In the 16th week after DMM, the right knee joints of mice were collected and fixed with 4 % paraformaldehyde overnight, decalcified with a formic acid solution (for further safranin O/fast green staining) for 1 week or EDTA solution (for further immunohistochemistry staining) for 4 weeks, dehydrated, embedded in paraffin, and cut into serial sagittal sections at 5- μ m thickness. The sections were stained with safranin O/fast green for morphological analysis. As previously mentioned [20], Osteoarthritis Research Society International (OARSI) score, cartilage area, synovitis score, osteophyte size and osteophyte maturity by blinded observers to assess the severity of OA-like phenotype.

2.10. Micro-CT analysis

Micro-computed tomography (Micro-CT) was used to analyze the bone defect and osteophyte formation in the knee joint of OA mice. The right knee was fixed in 4 % formaldehyde in mice for the night and cleaned with PBS before scanning. According to the previous protocol [16,20], in short, Venus[®] Micro-CT scanner (Pingsheng Healthcare Shanghai Inc., Shanghai, China) with a power supply voltage of 90 kV, a current of 70 μ A, and a resolution of 10 μ m was used to scan the knee joint of mice. Images were reconstructed and analyzed using Avatar V1.6.6 software with the same thresholds and normalized parameters for all samples. The calcified meniscus and osteophyte formation were quantified in mice. The area from the subchondral bone of the medial tibia to the growth plate was selected to analyze the medial subchondral bone density (sBMD) and medial subchondral bone volume per tissue volume (% sBV/TV). The region from tibial metaphysis to 1 mm below the growth plate and the region from 1 mm to 2 mm below the growth plate were selected. Free-shaped regions of interest (ROIs) were drawn, and multiple trabecular bone and cortical bone parameters were quantified and trabecular bone density (BMD), trabecular bone volume per tissue volume (BV/TV), trabecular number (Tb.N.), trabecular thickness (Tb.Th.), trabecular separation (Tb.Sp.), cortical bone density (cBMD) and cortical bone thickness (Ct.Th.) were measured.

2.11. Immunohistochemistry

After rehydration, sections from mouse knees were treated in antigen repair solution at 95 °C for 15 min. The sections were then treated with Endogenous Peroxidase Blocking Buffer (Beyotime, China) for 10 min and 0.5 % of Triton X-100 for 15 min, at 37 °C with goat serum blocking solution for 30 min. Further incubation with primary antibodies were performed overnight at 4 °C. After washing three times with PBST, sections were incubated with the corresponding secondary antibodies for 1h at room temperature, followed by treatment with Vectastain Elite ABC Kit (Vector Labs, Burlingame, CA). Immunohistochemistry (IHC) signals were revealed by ImmPACT DAB Peroxidase Substrate. The integrated optical density (IOD) value of positive staining was evaluated using Image J software (National Institutes of Health, MD, USA). The antibodies used in this study were listed in Table S1.

2.12. Proteomic profiling studies

P2 chondrocytes were cultured to 80 %–90 % confluence, starved for 6 h in the absence of FBS, and treated with TNF- α (20 ng/mL; 315-01B; PeproTech) for 12 h followed by 9 h with or without MSAB (50 μ M) for Proteomic profiling studies according to the manufacturer's instructions (LC-Bio Technology, China). The MS/MS data were searched for protein sequences which were downloaded from Uniprot database.

2.13. Luciferase reporter assay

To identify the binding interaction of β -catenin with the DDR2 promoter and study its effects, a TCF-overexpression plasmid, luciferase reporter vectors containing the wild-type promoter region of DDR2 (WT-DDR2) and mutant promoter region of DDR2 (Mut-DDR2) were constructed (Vector Builder, China). TCF overexpression plasmid and WT-DDR2-luc or Mut-DDR2-luc constructs were transfected into chondrocytes, using Lipofectamine 3000 (Invitrogen, USA) as previously described [21]. After 24 h, the cells were treated with or without MSAB (50 μ M) for another 24 h. Luciferase activity was then measured according to the instructions of the Dual Luciferase Reporter Gene Assay Kit (Yeasen Biotechnology, Shanghai, China).

2.14. Lenti-virus infection

The DDR2 overexpression Lenti-virus (CMV-DDR2) was constructed by Obio Technology Co., Ltd. After screening the optimum multiplicity of infection (MOI), we chose MOI = 50 for the infection. ATDC5 cells were treated with TNF- α (20 ng/mL) for 12 h, then infected with CMV-DDR2 or Lenti-Control for 24 h, and MSAB (50 μ M) was added for 12 h. Total RNA and protein were extracted for subsequent experiments.

2.15. Statistics

All data were presented as the means \pm SD. Comparisons between the two groups were performed by the two-tailed Student's *t*-test. Comparisons among multiple groups were analyzed by the one-way (or two-way or three-way) analysis of variance (ANOVA) followed by Tucky post-hoc test. The results were visualized and analyzed by the GraphPad PRISM software. Statistical significance is indicated as **P* < 0.05, ***P* < 0.01, and ****P* < 0.001.

3. Results

3.1. MSAB alleviates TNF- α -induced chondrocytes injury through inhibition of β -catenin signaling

To investigate if MSAB could potentially treat OA, we added MSAB into ATDC5 cells (a chondrogenic cell line) with TNF- α treatment. By qRT-PCR analysis, we found that expression of *Mmp3*, *Mmp13*, *Adams4*, *Adams5* and *Col-X* mRNAs was increased by TNF- α treatment in chondrocytes and addition of MSAB significantly suppressed the expression of these cartilage matrix catabolic biomarker genes (Fig. 1A–E). We also performed a pulse-chase experiment. The result demonstrated that active β -catenin protein levels decreased quicker in MSAB treated group (Fig. S3). In addition, Western blot data also confirmed that the MMP13, ADAMTS4, ADAMTS5 protein levels were down-regulated in chondrocytes after MSAB treatment compared with TNF- α treatment alone (Fig. 1F).

It was reported that MSAB inhibits Wnt/ β -catenin signaling by promoting β -catenin degradation. However, there are no reports whether MSAB also inhibits Wnt/ β -catenin signaling in chondrocytes. Thus, we next evaluate the efficiency of MSAB in inhibition of Wnt/ β -catenin signaling in chondrocytes. Immunofluorescence (IF) results showed that the levels of active β -catenin were decreased about 65.7 % in chondrocytes with the treatment of TNF- α +MSAB compared with TNF- α

treatment (Fig. 1G and H). MSAB did not affect the levels of total β -catenin in chondrocytes (Fig. 1G and I). We then analyzed the downstream genes of Wnt/ β -catenin signaling and found that expression of *Runx2*, *Axin2* and *Dkk1* was decreased about 50 % and *Cnd1* mRNA was decreased about 88 % in chondrocytes with the treatment of TNF- α +MSAB compared with TNF- α treatment alone (Fig. 1J–M). Western blot data showed that TNF- α upregulated the protein levels of active β -catenin, Axin2, and MMP3 while MSAB significantly suppress levels of these proteins (Fig. 1N–Q).

In addition to evaluating the effects of MSAB on chondrocytes, we also investigated effects of MSAB on osteoblast and osteoclast function, as well as its impact on DRG cells. The results of Alizarin Red staining and the expression of osteoblast-related functional markers (*Alp*, *Runx2* and *Sp7*) demonstrated that MSAB has the inhibitory effect on osteoblast mineralization (Fig. S4). The results of TRAP staining and the expression of osteoclast-related functional markers (*Ctsk*, *Acp5* and *Mmp9*) showed the inhibitory effect of MSAB on osteoclast formation (Fig. S5). Taken together, our data suggest that MSAB has therapeutic potential against OA in *in vitro* experiments.

3.2. Serum albumin nanoparticles efficiently target chondrocytes

To efficiently deliver MSAB into OA mouse model, we used a human serum albumin nanoparticle (HSA-NP) system for the encapsulation and transport of MSAB. MSAB/HSA nanoparticles were constructed through HSA intermolecular disulfide bond remodeling by ultrasonication treatment (Fig. 2A). The obtained nanoparticles were measured by dynamic light scattering (DLS), and the mean particle sizes of the MSAB/HSA were increased approximately 16 nm (Fig. 2B). The zeta potential of the HSA-NPs and MSAB/HSA were -19.5 ± 0.3 mV and -24.7 ± 1.3 mV, respectively, indicating that MSAB was successfully bound to HSA-NPs, which indirectly proved the successful synthesis of MSAB/HSA (Fig. 2C). Meanwhile, transmission electron microscopy (TEM) images showed HSA-NPs and MSAB/HSA had well-defined spherical structures and the homogeneity of MSAB/HSA at approximately 75 nm, further confirming the size distribution of MSAB/HSA (Fig. 2D). To investigate the release of MSAB/HSA, we measured the drug release kinetics of nanoparticle in a natural environment from 0 h to 72 h. As expected, the acceleration of MSAB drug release was observed within 24 h and then peaked after 48 h (Fig. 2E), indicating good stability and sustained release of the HSA nanoparticles. Next, we used an *in vivo* imaging tracking system to detect HSA-NP duration *in vivo* and found that ICG-labeled HSA-NP persisted for at least 3 days after a single intra-articular injection (Fig. 2F and G). To further determine whether HSA could be efficiently uptaken by chondrocytes, we used dil probe to stain the cell membrane and added HSA-NP-ICG into ATDC5 cells. IF staining showed that HSA-NP-ICG could enter ATDC5 cells (Fig. 2H). These findings indicate that intra-articular injection of MSAB/HSA may efficiently target chondrocytes and cartilage tissue.

3.3. MSAB/HSA improves OA related pain in OA mouse model

To determine whether MSAB/HSA could alleviate OA pain, we performed DMM surgery on 10-week-old C57/BL6 mice to establish OA mouse model, and then intra-articular injected OA mice with MSAB/HSA twice a week (Fig. S2). There were no significant changes in histological differences and pain-related behaviors between MSAB/HSA and vehicle treatment group in WT mice without DMM surgery (Figs. S6–S8). The IHC results demonstrated that the expression of the active β -catenin, total β -catenin and Wnt/ β -catenin signaling downstream molecule Axin2 were significantly decreased in DMM mice after treatment with MSAB/HSA (Figs. S9 and S10). The pain-related spontaneous activity of mice was evaluated by LABORAS™ analyses. We found that MSAB/HSA-treated mice showed a significant increase in the motion track record compared to the OA mice without MSAB treatment (Fig. 3A). The average walking speed (Fig. 3B), travel distance (Fig. 3C),

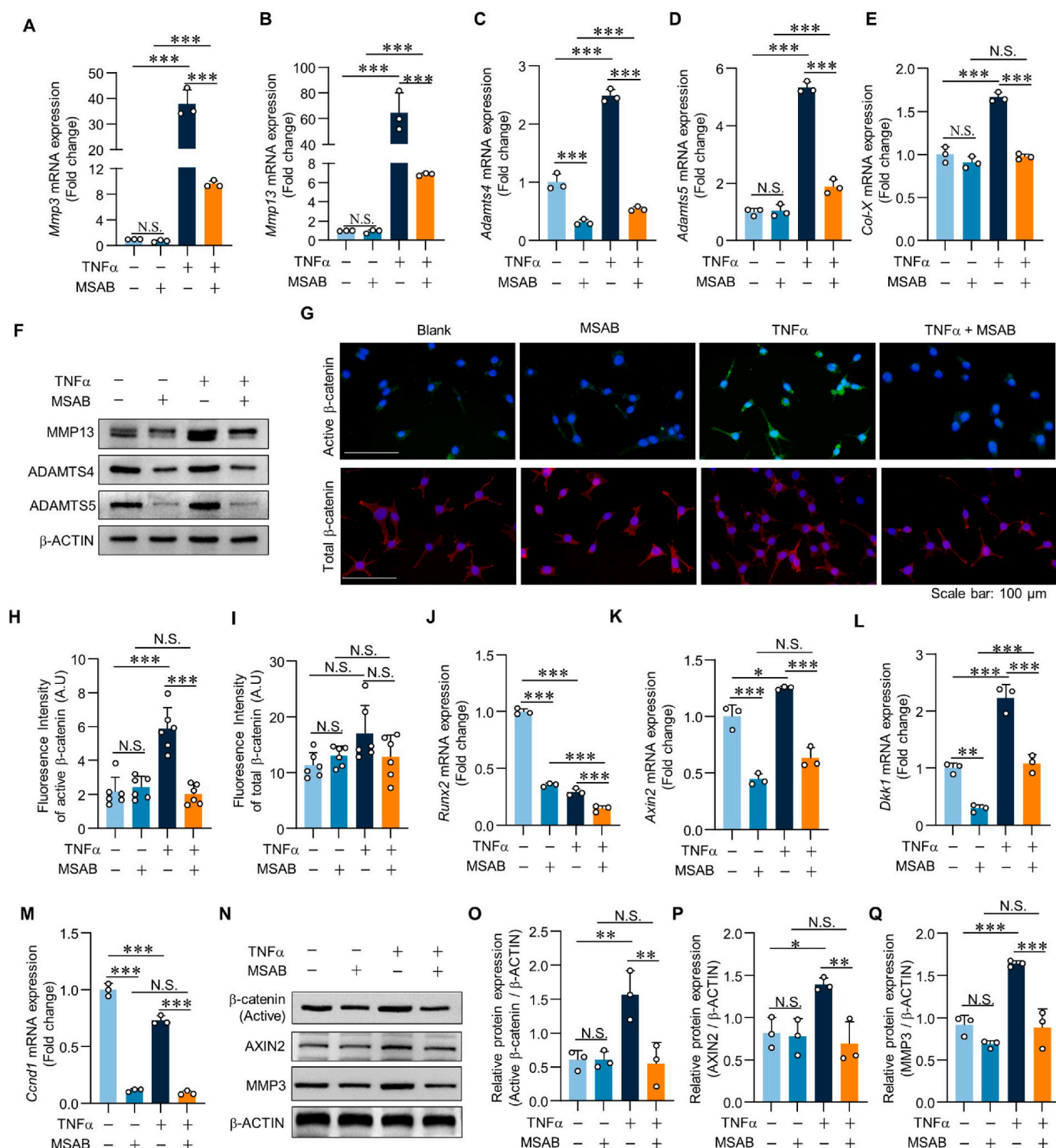


Fig. 1. MSAB alleviates TNF- α -induced chondrocytes injury through inhibition of β -catenin signaling. (A–E) qRT-PCR was performed to examine changes in mRNA expression of *Mmp3* (A), *Mmp13* (B), *Adamts4* (C), *Adamts5* (D) and *Col-X* (E) in ATDC5 cells as indicated (n = 3). (F) Expression of MMP13, ADAMTS4 and ADAMTS5 proteins was detected by Western blotting in ATDC5 cells treated with TNF- α or MSAB as indicated (n = 3). (G–I) Representative IF images (G) showing active β -catenin (non-phosphorylated β -catenin) and total β -catenin expression. Quantification of fluorescence intensity of active β -catenin (H) and total β -catenin (I) in ATDC5 cells treated with TNF- α or MSAB (n = 6). (J–M) The mRNA expression of *Runx2* (J), *Axin2* (K), *Dkk1* (L) and *Ccnd1* (M) in ATDC5 cells was detected by qRT-PCR (n = 3). (N–Q) Representative immunoblots (N) and quantification of active β -catenin (O), AXIN2 (P), and MMP3 (Q) expression in ATDC5 cells treated with TNF- α or MSAB as indicated (n = 3). * P < 0.05, ** P < 0.01, *** P < 0.001, N.S.: no significant difference. Data are represented as mean \pm SD. Statistical differences were analyzed by one-way ANOVA followed by the Tukey post-hoc test (A–E, H–M and O–Q).

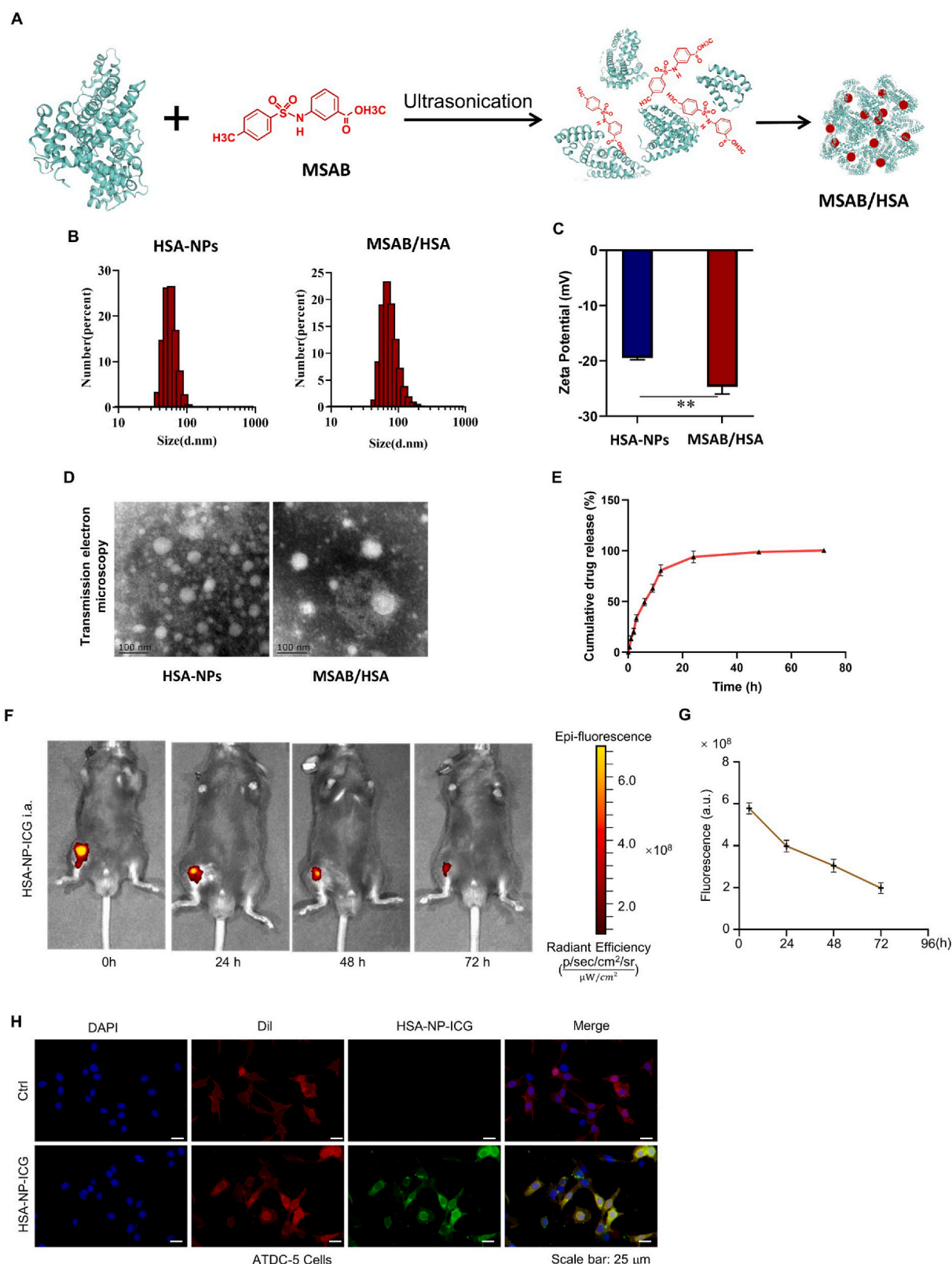


Fig. 2. Serum albumin nanoparticles efficiently target chondrocytes. (A) A schematic diagram illustrating HSA loaded with MSAB. (B) The size distribution and (C) apparent Zeta potential of HAS-NPs and MSAB/HSA. (D) The representative images of transmission electron microscopy of HAS-NPs and MSAB/HSA (E) Cumulative drug release of MSAB delivered by HSA in PBS ($n = 3$) (F and G) Tracking HSA-NP-ICG after intra-articular injection with *in vivo* imaging (F) and quantification (G). HSA-NP-ICG was detected after intra-articular injection by *in vivo* imaging in the time points as indicated. (H) Representative IF images showing HSA-NP-ICG enter into the ATDC5 cells and are located in the cytoplasm. Purified HSA-NP were labeled with Purified from the dye ICG. Dil was used to stain the cell membranes. DAPI was used to stain the nuclei. Data were analyzed by two-tailed Student's *t*-test analysis (C).

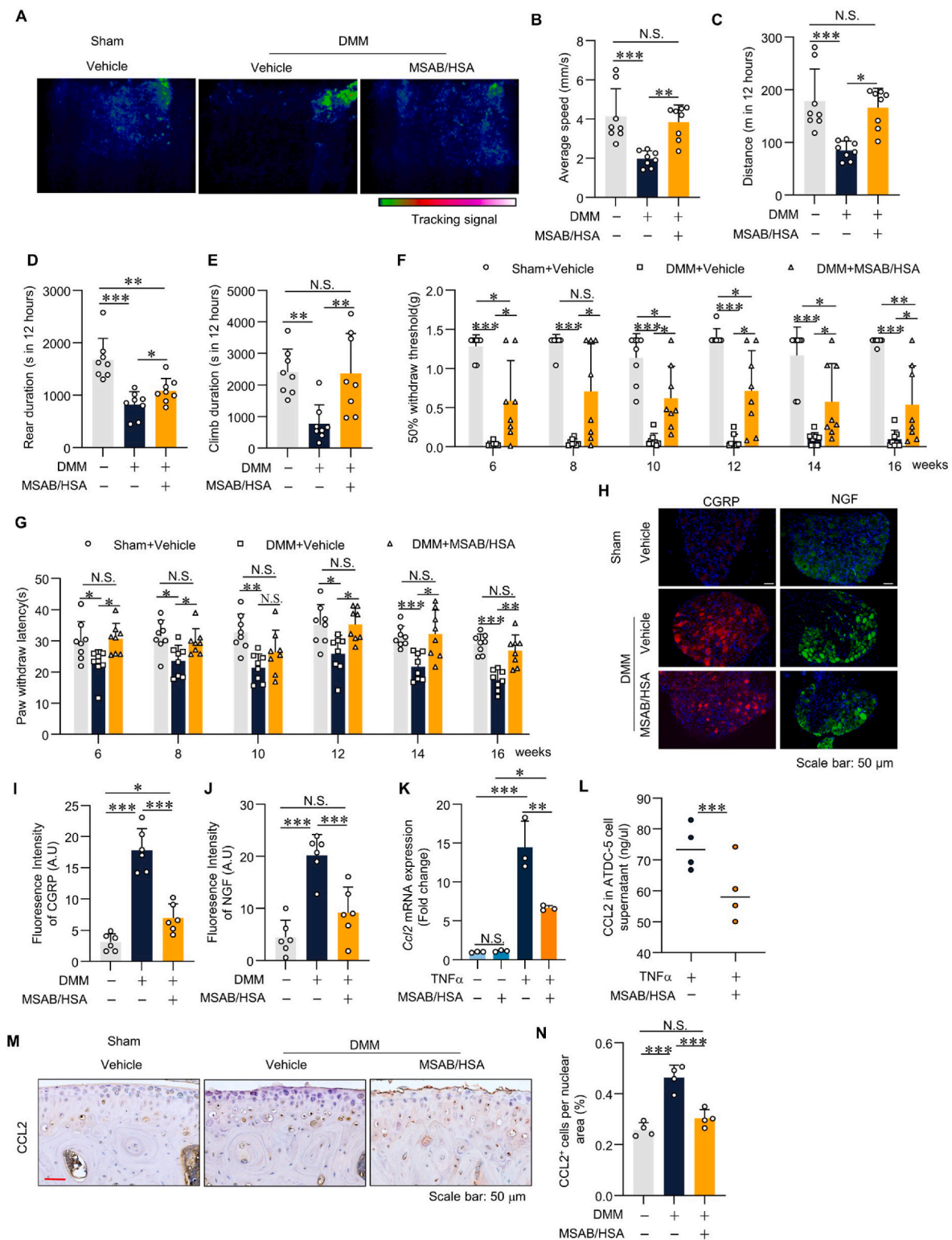


Fig. 3. MSAB/HSA improves OA related pain in OA mouse model. (A–E) The representative images of the motion track record of the mice (A), average speed (B), distance (C), rearing duration (D), and climb duration (E) in mouse groups as indicated ($n = 8$). (F) The von Frey test showed the sensitivity to mechanical allodynia in the mice with Sham operation or DMM surgery treated with Vehicle or MSAB/HAS in the time points as indicated ($n = 8$). (G) The hotplate test showed the sensitivity to thermal hyperalgesia in the mice with Sham operation or DMM surgery treated with Vehicle or MSAB/HSA in the time points as indicated ($n = 8$). (H, I and J) Representative IF images (H) showed CGRP and NGF expression and quantitative fluorescence intensity of CGRP (I) and NGF (J) in dorsal root ganglia (DRG) in the mice with Sham operation or DMM surgery treated with Vehicle or MSAB/HSA ($n = 6$). (K) qRT-PCR was performed to examine changes in the relative mRNA expression of *Ccl2* (K) in different groups of ATDC5 cells ($n = 3$) as indicated. (L) Secreted CCL2 level in ATDC-5 cell treated with TNF- α or MSAB/HSA as indicated ($n = 4$) (M–N) Representative IHC images (M) (scale bar 50 μ m) showing expression of CCL2⁺ (N) cells in cartilage area of in the mice with Sham operation or DMM surgery treated with Vehicle or MSAB/HSA ($n = 4$). * $P < 0.05$, ** $P < 0.01$, *** $P < 0.001$, N.S.: no significant difference. Data are represented as mean \pm SD. Statistical differences were analyzed by one-way (or two-way) ANOVA followed by the Tukey post-hoc test (B–G, I–K and N) and by two-tailed Student's *t*-test (L).

rear duration (Fig. 3D), climb duration (Fig. 3E), rear frequency (Fig. S11A) and climb frequency (Fig. S11B) were also significantly improved in MSAB/HSA-treated group compared with vehicle-treated OA group. We then performed von Frey test and hotplate test to assess mechanical allodynia and thermal nociceptive sensitivity in OA mice treated with or without MSAB/HSA. DMM-induced OA mice showed a lower von Frey score (reflecting increased pain sensitivity), which can be partially reversed by the treatment with MSAB/HSA (Fig. 3F). In addition, MSAB/HSA treatment also improved thermal allodynia in OA mice (Fig. 3G). OA related pain signaling was mediated by dorsal root ganglion (DRG). Thus, we performed IF staining to determine the activation of DRG after MSAB/HSA treatment in OA mice and found that calcitonin gene-related peptide (CGRP) and nerve growth factor (NGF) positive signals were upregulated after DMM surgery, while MSAB/HSA could inhibit CGRP expression by 61 % and inhibit NGF expression by 54 % in OA mice (Fig. 3H–J). Further, our previous studies demonstrated that β -catenin-TCF7 activates the transcription of CCL2, a known key factor mediating pain hypersensitivity in OA [7]. We also evaluated CCL2 expression in ATDC5 cells with TNF- α or MSAB treatment, and found that MSAB inhibited *Ccl2* mRNA expression compared with the effects of TNF- α treatment alone (Fig. 3K). Through ELISA analysis, we observed that MSAB/HSA treatment can inhibit the secretion of CCL2 in ATDC5 cells following TNF- α stimulation (Fig. 3L). Additionally, IHC analysis revealed a decrease in the number of CCL2-positive chondrocytes after treatment with MSAB/HSA (Fig. 3M and N). We also perform co-culture of primary chondrocytes treated with TNF- α with or without MSAB/HSA and primary DRGs to investigate their effects on DRG functional parameters and axon growth. Interestingly, the results of co-culture experiments showed a significant down-regulation of pain-related neural markers in DRGs (*TrpV1*, *Calca*, *Ngf*) (Fig. S12). These findings suggest that the alleviation of OA pain by MSAB may be through its impact on chondrocytes, indirectly influencing pain signal transduction. Taken together, MSAB could promote β -catenin degradation to inhibit β -catenin-TCF7 signaling and subsequently relieve pain signaling transmission in DRG.

3.4. MSAB/HSA alleviates cartilage degradation in DMM-induced OA mice

We next investigated whether MSAB/HSA can alleviate cartilage degradation in DMM-induced OA mice. Safranin O/Fast Green staining was used to assess severity of defects in articular cartilage and OARSI scores (a semi-quantitative measure of OA) after DMM surgery. We found MSAB/HSA significantly attenuated cartilage degeneration in DMM-induced OA mice compared with OA mice without MSAB/HSA treatment, and the treatment with MSAB/HSA decreased the OARSI score about 37 % (Fig. 4A and B). Further histological analysis indicated cartilage area was recovery in MSAB/HSA treatment group (Fig. 4C). Prominent synovial hyperplasia (Fig. 4D) and osteophyte formation (Fig. 4E and F) analyzed by synovitis score and osteophyte size and maturity were observed in mice at 16 weeks after DMM surgery, and these effects were significantly inhibited by the MSAB/HSA treatment after DMM surgery. Micro-CT analysis also confirmed decreased osteophyte formation in MSAB/HSA treated group compared with vehicle treated group after DMM surgery (Fig. 4G and H). To evaluate the effect of MSAB/HSA on bone mass in OA mice, the medial subchondral bone, trabecular bone, and cortical bone were analyzed separately (Fig. 4I). We observed a significant increase in medial subchondral bone mineral density (sBMD) and subchondral bone per unit tissue volume (% sBV/TV) in the mice 16 weeks after DMM surgery, and mice treated with MSAB/HSA following DMM surgery exhibited lower sBMD (approximately 11 % reduction) and sBV/TV (approximately 23 % reduction) compared with OA mice treated with vehicle (Fig. 4J and K). In addition, trabecular bone density (tBMD), trabecular bone volume per tissue volume (tBV/TV), trabecular number (Tb.N.), trabecular thickness (Tb.Th.), trabecular separation (Tb.Sp.), cortical bone mineral density

(cBMD) and cortical bone thickness (Ct.Th.) showed no statistical differences in OA mice treated with or without MSAB/HSA (Fig. S13). Next, we performed IHC to determinate whether MSAB/HSA can affect extracellular matrix synthesis and catabolism in chondrocytes. We found that MSAB/HSA treatment significantly suppressed MMP13 expression and promoted Col-2 expression in DMM mice (Fig. 4L–N). We also assessed whether HSA could enhance the effect of MSAB. Results of Safranin O/Fast Green staining revealed that DMM mice treated with MSAB/HSA had lower OARSI scores compared to the group treated with MSAB alone (Figs. S14A–S14B). The IHC results showed that in the MSAB/HSA treatment group, mice exhibited a larger Acan-positive cartilage area compared to the group treated with MSAB alone (Figs. S14C–S14D).

3.5. MSAB decreases DDR2 expression in OA

To further investigate the protective mechanism of MSAB in OA, we performed LC-MS/MS-based proteomics analysis on primary chondrocytes treated with TNF- α +MSAB/HSA or TNF- α +vehicle. 57 up-regulated and 40 down-regulated proteins were identified in chondrocytes treated with MSAB (Fig. 5A). And majority of significant changed proteins located in cytoplasm and nucleus (Fig. 5B). The EggNOG analysis showed candidate proteins identified in the mice with MSAB/HSA treatment were mainly involved in intracellular trafficking, secretion, and vesicular transport signaling (Fig. 5C). To screen the candidate(s) that could be regulated by MSAB in OA mice, we used a volcano plot visualization technique to evaluate differentially expressed proteins in primary chondrocytes treated with TNF- α +MSAB/HSA vs TNF- α +vehicle (Fig. 5D), and base on literature search, DDR2 was identified for further investigation. DDR2 expression in MSAB treated group decreased about 56 % compared with Ctrl group in proteomic assay (MSAB vs Ctrl = 0.44132914, *P* value = 0.0435). We then performed qRT-PCR, Western blot and IHC to determinate DDR2 expression using *in vitro* or *in vivo* OA models. We found *Ddr2* mRNA expression was significantly decreased in ATDC5 cells treated with TNF- α +MSAB/HSA compared to the chondrocytes treated with TNF- α +vehicle (Fig. 5F). The results of Western blot demonstrated that the expression of DDR2 protein was significantly increased in chondrocytes treated with TNF- α , and the treatment with MSAB/HSA down-regulated DDR2 expression (Fig. 5G). The IHC results showed that DDR2 levels were increased in chondrocytes of DMM mice and treatment with MSAB/HSA significantly decreased DDR2 expression chondrocytes (Fig. 5H and I). Consistently, IF results also showed the similar results (Figs. S15A–S15B).

3.6. MSAB decrease DDR2 expression by inhibiting β -catenin signaling

To determine how MSAB regulates the DDR2 expression in OA, we constructed wild-type (WT) and mutant (Mut) DDR2-promoter constructs (Fig. 6A) and performed luciferase reporter assay. We found that the relative luciferase activity was significant decreased after MSAB treatment compared with WT DDR2-Luc construct transfected group, while co-transfected with TCF7 plasmids could partially rescue the reduced luciferase activity (Fig. 6B). Additionally, transfection with Mut1 DDR2-promoter constructs (Mut1 sites: 879/-868) also decreased relative luciferase activity, but Mut2 DDR2-promoter constructs (Mut2 sites: 567/-556) showed no effect on the luciferase activity (Fig. 6C). To further confirm the protective effect of MSAB on OA was mediated by DDR2, we used lentivirus CMV-Ddr2 to overexpress *Ddr2* in chondrocytes (Fig. S16). We found that *Mmp13* mRNA and protein levels were partially reversed in MSAB treated chondrocytes with CMV-Ddr2 infection (Fig. 6D–G). IF staining also confirm these results that TNF- α induced high MMP13 expression in chondrocytes, while MSAB significantly attenuated these effects, and MMP13 expression was recovered after CMV-Ddr2 infection (Fig. 6H and I). We activated the β -catenin signaling pathway in chondrocytes by BIO to induce elevated expression of *Mmp13* and *Adams5*. Subsequently, *Ddr2* siRNA was used to inhibit

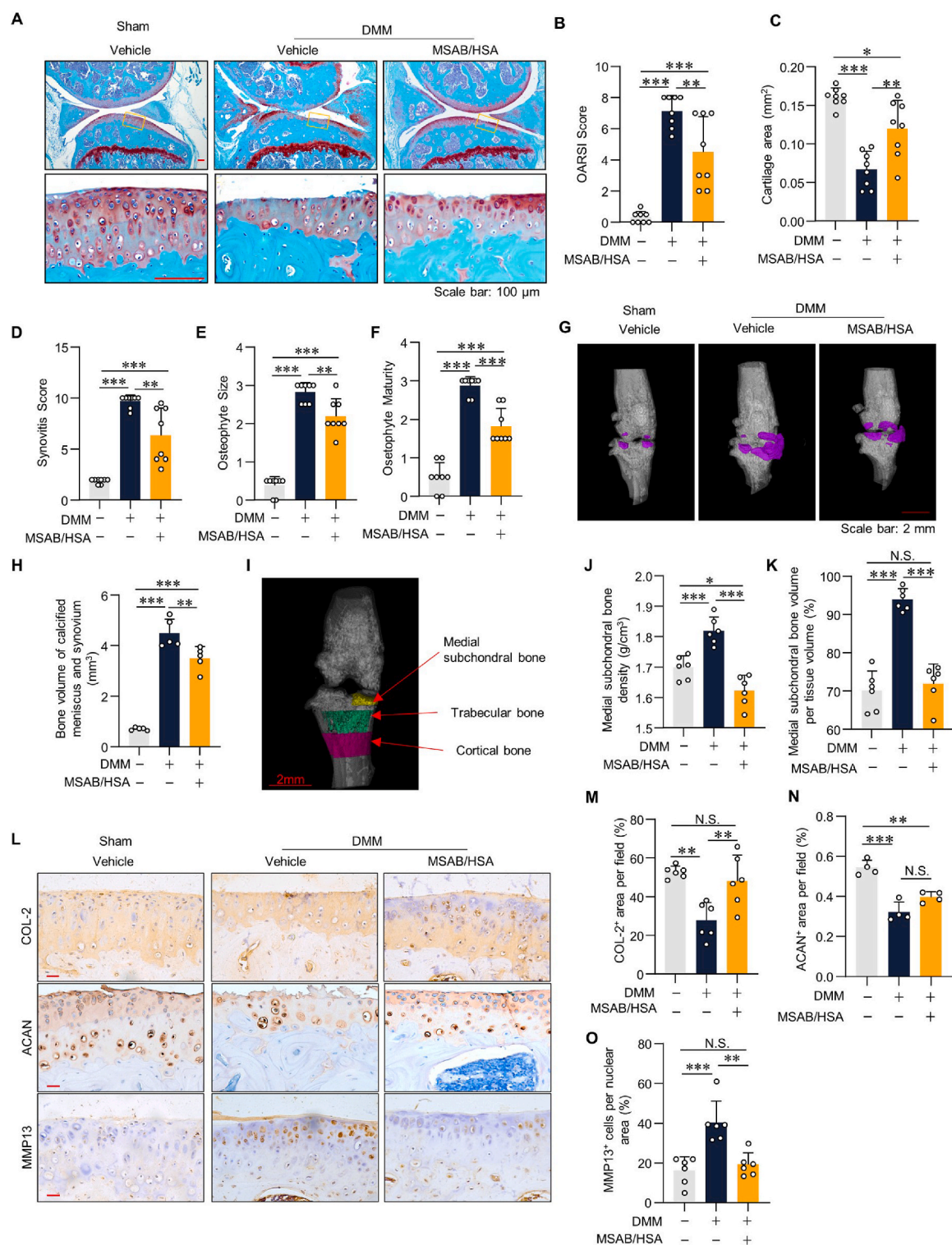


Fig. 4. MSAB/HSA alleviates cartilage degradation in DMM-induced OA mouse model. (A–F) Representative Safranin O/Fast green staining images (A) (scale bar 100 μ m) and analysis of OARSI scores (B), cartilage area (C), synovitis scores (D), osteophyte size (E) and osteophyte maturity (F) in the mice with Sham operation or DMM surgery treated with Vehicle or MSAB/HSA ($n = 8$). (G and H) Micro-CT representative images (G), and bone volume of calcified meniscus and synovium (Purple markers) quantifications (H) in the mice with Sham operation or DMM surgery treated with Vehicle or MSAB/HSA ($n = 5$). (I) A schematic diagram showed the region of interest (ROI) selected to quantify the relevant indicators. ROI: medial subchondral bone (yellow); trabecular bone (green); cortical bone (pink). (J and K) Quantification of medial subchondral bone mineral density (J) and medial subchondral bone volume per tissue volume (K) of the mice with Sham operation or DMM surgery treated with Vehicle or MSAB/HSA ($n = 6$). (L–P) Representative IHC images (L) (scale bar 25 μ m) showing expression of COL-2⁺ (M) cells, ACAN⁺ (N) area and MMP13⁺ (O) cells in cartilage area of in the mice with Sham operation or DMM surgery treated with vehicle or MSAB/HSA ($n = 6$). * $P < 0.05$, ** $P < 0.01$, *** $P < 0.001$, N.S.: no significant difference. Data are represented as mean \pm SD. Statistical differences were analyzed by two-way ANOVA followed by the Tukey post-hoc test (B–F, H, J, K, M – O).

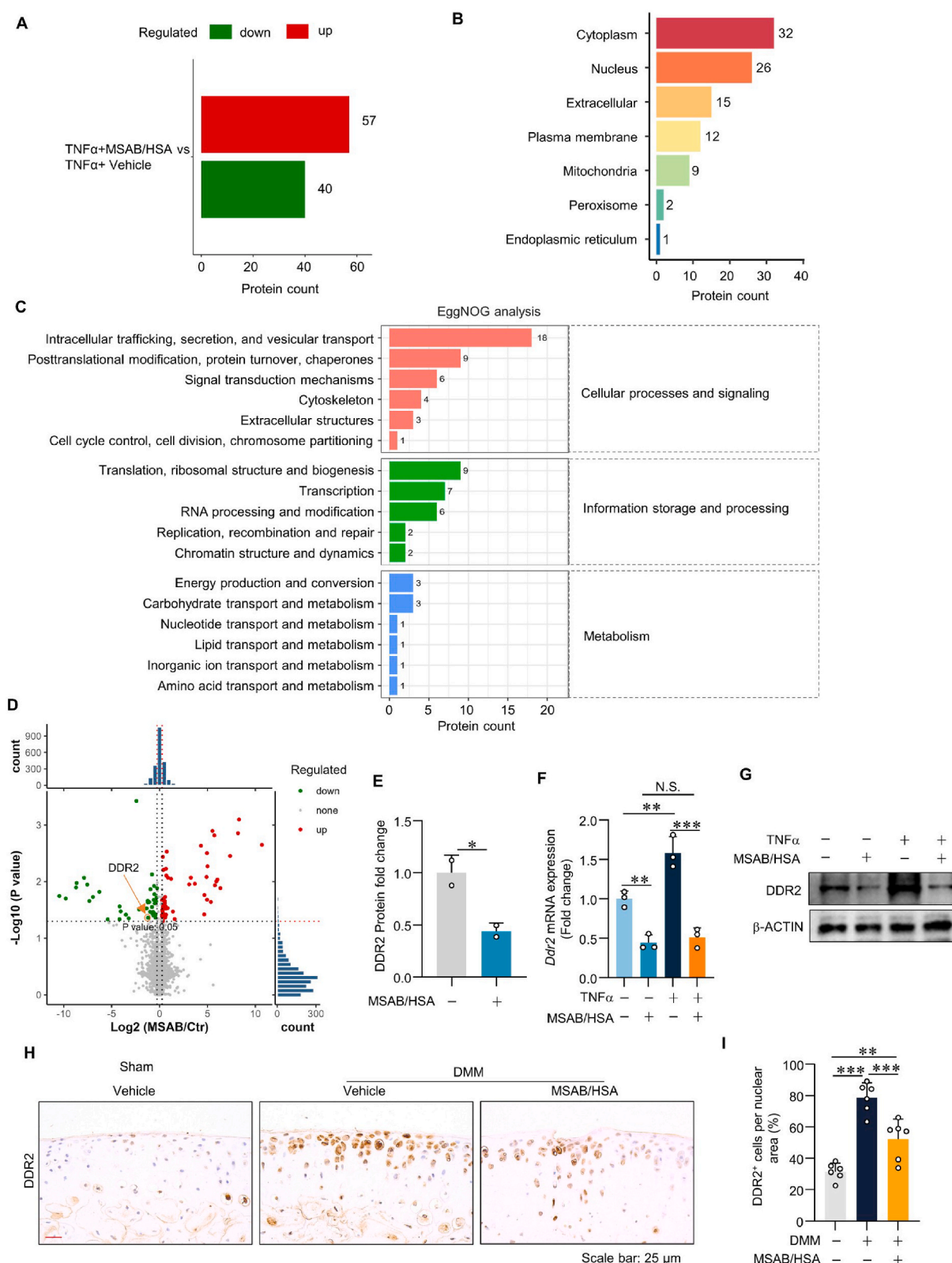


Fig. 5. MSAB decreases DDR2 expression in OA. (A–C) The number (A), location (B) and EggNOG analysis (C) of changed proteins in primary chondrocytes treated with TNF- α +MSAB/HSA vs TNF- α +Vehicle. (D)Volcano plot analysis showed DDR2 was down-regulated in primary chondrocytes treated with TNF- α +MSAB/HSA compare with the cells treated with TNF- α +Vehicle. (E) Fold changes in DDR2 expression in MSAB treated group compared with PBS treated group (n = 2 paired biological replicates). (F) qRT-PCR was performed to examine the relative *Ddr2* mRNA levels in different groups of ATDC5 cells treated as indicated (n = 3). (G) Representative Western blot data of DDR2 expression in ATDC5 cells treated with MSAB. (G and H) Representative IHC images (H) (scale bar 25 μm) showing expression of DDR2 $^{+}$ (I) cells in the cartilage area of the mice with Sham operation or DMM surgery treated with Vehicle or MSAB/HSA (n = 6). * P < 0.05, ** P < 0.01, *** P < 0.001, N.S.: no significant difference. Data are represented as mean \pm SD. Two group of data were analyzed by two-tailed Student's *t*-test (E). Comparisons of data with multiple groups were analyzed by two-way ANOVA followed by the Tukey post-hoc test (F and I).

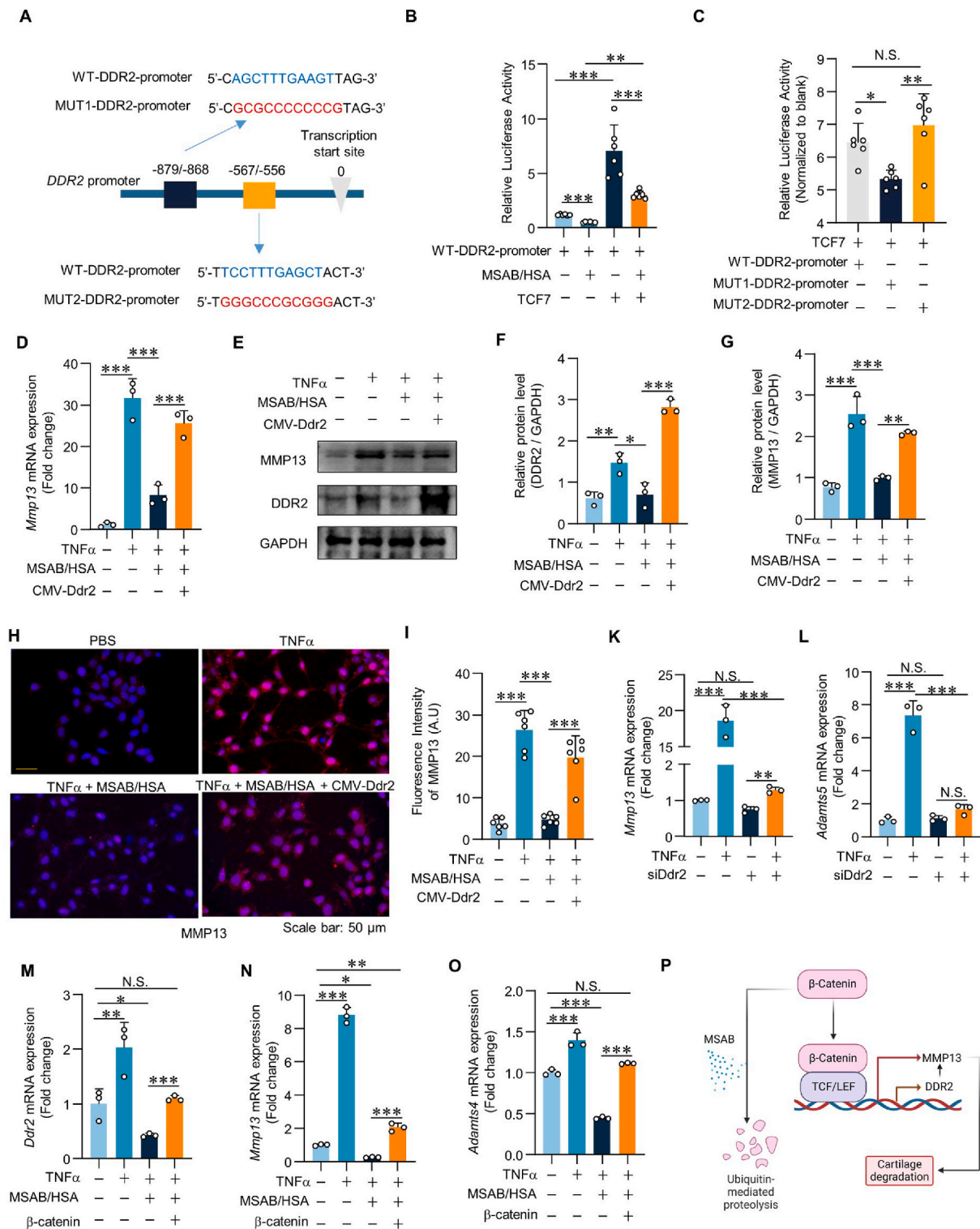


Fig. 6. MSAB decreases DDR2 expression by inhibiting β -catenin signaling. (A) A schematic diagram indicated the mutation sites of DDR2 luciferase reporter constructs. (B and C) DDR2 luciferase activity of different groups as indicated, with the level in the blank group arbitrarily set to 1. (D) qRT-PCR was performed to examine the relative *Mmp13* mRNA levels of different groups of ATDC5 cells as indicated ($n = 3$). (E, F and G) Representative immunoblots (E) and quantification of DDR2 (F) and MMP13 (G) expression in ATDC5 cells with CMV-DDR2 infection ($n = 3$). (H and I) Representative IF images (H) showing MMP13 and quantification of MMP13 fluorescence intensity (I) in ATDC5 cells with CMV-DDR2 infection ($n = 6$). (K and L) qRT-PCR was performed to examine changes in the relative mRNA expression of *Mmp13* (K) and *Adamts5* (L) in ATDC5 cells treated as indicated. (M–O) qRT-PCR was performed to examine changes in the relative mRNA expression of *Ddr2* (M), *Mmp13* (N) and *Adamts4* (O) in ATDC5 cells treated as indicated ($n = 3$) (P) A schematic diagram showed the mechanism by which MSAB decreases cartilage degradation. * $P < 0.05$, ** $P < 0.01$, *** $P < 0.001$, N.S.: no significant difference Data are represented as mean \pm SD. Statistical differences were analyzed by two-way ANOVA followed by the Tukey post-hoc test (B–D, F, G, I–L and M – O).

Ddr2 expression in chondrocytes. The results showed that *Ddr2* siRNA could partially alleviate the increase of metalloproteinases following β -catenin signaling activation in chondrocytes (Fig. 6K and L). Moreover, in the cell culture in which MSAB/HSA inhibited the expression of *Ddr2*, *Mmp13* and *Adams4* in chondrocytes and overexpression of β -catenin could also partially reverse the therapeutic effects of MSAB/HSA (Fig. 6M–O). Taken together, MSAB exerts its chondro-protective effect by inhibition of β -catenin-DDR2 signaling (Fig. 6P).

4. Discussion

The enzymatic degradation of collagen and proteoglycan by Matrix Metalloproteinases (MMPs) and A Disintegrin and Metalloproteinase with Thrombospondin Motifs (ADAMTS) is the critical event to the molecular pathology of OA [8,9]. The aberrant activation of Wnt/ β -catenin signaling, which results in elevated expression of MMPs and ADAMTS, has been recognized as a significant contributor to OA pathogenesis [22–24]. Thus, targeting the hyperactivated Wnt/ β -catenin pathway offers a promising therapeutic avenue for OA management [25–27]. To date, various strategies targeting β -catenin have been developed, falling into three principal categories: modulating receptor signaling, disrupting complex assembly, and influencing gene transcription [28–30]. Notable among these are indirect methods, principally involving therapeutic agents that modulate upstream effectors of the Wnt/ β -catenin pathway. Reports indicate that intra-articular injections of small molecule inhibitors like XAV-939 and C113 ameliorate OA symptoms and reduce joint cartilage deterioration and synovitis in OA animal models [31]. Additionally, other inhibitors such as SAH-Bcl9 and StAx-35R have been shown to arrest the transformation of aberrant chondrocyte phenotype, thereby preserving early-stage OA development. This is evidenced by the upregulation of *Sox9* and *Acan* genes and downregulation of *Col-X* [32]. *Sox9* plays a critical role of chondrocyte development and cartilage tissue homeostasis [33]. The role of MSAB on *Sox9* expression needs to be further investigated. Our previous finding has identified that the β -catenin/TCF inhibitor iCRT14 markedly diminishes MMP13, Col-X, and *Adams5* expression in the mice with spinal degeneration after lumbar spine instability (LSI) surgery. The key regulatory mechanism for β -catenin activity is the phosphorylation mediated ubiquitin-proteasome degradation mechanism. The novel inhibitor MSAB, which selectively binds to the armadillo domain of β -catenin has been shown to facilitate β -catenin ubiquitination and subsequent proteasomal degradation [34,35]. In oncological models, MSAB has been demonstrated to decrease tumor mass and induce apoptosis in Wnt-dependent neoplasms [34,36]. *In vitro* studies reveal that MSAB treatment substantially curtails Wnt/ β -catenin signaling, reducing the mRNA and protein levels of MMP13 and ADAMTS5 in TNF- α -stimulated chondrocytes. Furthermore, MSAB complexed with Human Serum Albumin (MSAB/HSA) has been shown to effectively mitigate cartilage degeneration in OA animal models.

To enhance the delivery efficacy of MSAB, we employed HSA for its nanoparticulate transport into chondrocytes. HSA, a soluble globular protein composed of 585 amino acid residues and a molecular weight of 66,500 Da, features a single sulfhydryl group and 17 disulfide bridges within its structure [37]. The application of HSA in nanoparticle-based drug delivery systems is advantageous due to its preferential tissue uptake, biodegradability, and non-toxic nature, particularly in neoplastic and inflamed tissues [38–41]. Studies have demonstrated the capacity of HSA nanoparticles to deliver therapeutic agents like nioscapine with precision, optimizing therapeutic efficacy and minimizing side effects [42]. Analogous research has revealed the potency of HSA nanoparticles in targeting neoplasms with cytokines and chemotherapeutic agents, amplifying anti-cancer effects while curtailing toxicity [43,44]. In this study, MSAB was encapsulated within HSA-based nanoparticles (HSA-NPs) to facilitate efficient intracellular delivery and enhance bioavailability. Future work will focus on evaluating a broader spectrum of delivery matrices and conducting comparative analyses to ascertain

the most effective and safe MSAB delivery for OA therapy. Furthermore, this study found that HSA-NP tagged with Indocyanine Green (ICG) could target chondrocytes and remain within the articular cartilage tissue for an extended period, suggesting favorable biostability and biosafety profiles. However, the potential reparative effects of HSA nanoparticles alone on cartilage were not assessed. Subsequent studies will be aiming at comparing the therapeutic impact of HSA and MSAB-conjugated HSA (MSAB/HSA) on cartilage repair, prevention of osteophyte formation, and alleviation of OA-related pain.

Previous investigations have identified an upregulation of DDR2 in the chondrocytes of human OA [45] and in the fibroblast-like synoviocytes characteristic of rheumatoid arthritis [46]. The DDR2/annexin A2/MMP 13 axis has been implicated in exacerbating joint damage in arthritic conditions by facilitating the migration and invasion of synoviocytes [47]. Activation of DDR2 in OA contexts has been associated with enhanced MMP13 expression, culminating in cartilage breakdown [48,49]. In the present studies, we have demonstrated that MSAB complexed with HAS (MSAB/HSA) is capable of mitigating DDR2 activation, thereby impeding MMP13 induction and attenuating OA progression. Additionally, our research delineates the interplay between the Wnt/ β -catenin signaling pathway and DDR2, revealing that MSAB mediates the downregulation of DDR2 transcription through the inhibition of β -catenin signaling, resulting in reduced MMP13 levels and consequent cartilage preservation.

In conclusion, the current findings indicate that HSA may serve as an effective vector for MSAB delivery in OA therapy, with the amelioration of cartilage deterioration attributable to the suppression of β -catenin-DDR2 signaling. These insights offer a promising new approach to treat both the symptomatic and structural defects of OA.

CRediT authorship contribution statement

Ke Lu: Writing – original draft, Validation, Investigation, Funding acquisition, Data curation. **Zhidong Liao:** Writing – original draft, Methodology, Investigation, Formal analysis, Data curation. **Jingwen Li:** Investigation, Formal analysis, Data curation. **Yuhan Wang:** Methodology, Investigation, Data curation. **Yuting Zhang:** Methodology, Investigation. **Lintao Cai:** Visualization, Validation, Supervision. **William W. Lu:** Writing – review & editing, Supervision, Funding acquisition. **Fan Yang:** Writing – review & editing, Validation, Supervision. **Hong Pan:** Writing – original draft, Validation, Resources. **Di Chen:** Writing – review & editing, Supervision, Project administration, Funding acquisition, Conceptualization.

Data availability statement

The data that support the findings of this study are available in the main text or the supplementary materials or from the corresponding author upon reasonable request.

Ethics approval and consent to participate

The animal protocol of this study has been approved by Ethics Committee of the Shenzhen Institute of Advanced Technology, Chinese Academy of Sciences and all experimental methods and procedures were carried out in accordance with the approved protocol to comply with all ethical regulations for animal testing and research (SIAT-IACUC-210618-YY-CD-A1955). The current study does not involve human subject participation.

Funding information

This project was supported by the National Natural Science Foundation of China (NSFC) grants 82394445, 82250710174, 82161160342, and 82030067 to D.C. and grant 82302757 to K.L. This project was also supported by the Hong Kong RGC grant HKU-17101821 to W.W.L. and

D.C. and SIAT Innovation Program for Excellent Young Researchers to K. L.

Declaration of competing interest

The authors declare that they have no known competing financial interests or personal relationships that could have appeared to influence the work reported in this paper.

Appendix A. Supplementary data

Supplementary data to this article can be found online at <https://doi.org/10.1016/j.bioactmat.2024.10.023>.

References

- [1] D. Chen, J. Shen, W.W. Zhao, T.Y. Wang, L. Han, J.L. Hamilton, H.J. Im, Osteoarthritis: toward a comprehensive understanding of pathological mechanism, *Bone Res* 5 (2017) 16044.
- [2] L.P. Tong, H. Yu, X.Y. Huang, J. Shen, G.Z. Xiao, L. Chen, H.Y. Wang, L.P. Xing, D. Chen, Current understanding of osteoarthritis pathogenesis and relevant new approaches, *Bone Res* 10 (1) (2022) 60.
- [3] L. Tong, A.J.v. Wijnen, H. Wang, D. Chen, Advancing bone biology: the mutual promotion of biology and pioneering technologies, *The Innovation Life* 2 (3) (2024) 100078.
- [4] C. Xia, P. Wang, L. Fang, Q. Ge, Z. Zou, R. Dong, P. Zhang, Z. Shi, R. Xu, L. Zhang, C. Luo, J. Ying, L. Xiao, J. Shen, D. Chen, P. Tong, H. Jin, Activation of beta-catenin in Col2-expressing chondrocytes leads to osteoarthritis-like defects in hip joint, *J. Cell. Physiol.* 234 (10) (2019) 18535–18543.
- [5] M. Wang, S. Li, W. Xie, J. Shen, H.J. Im, J.D. Holz, M. Wang, T.G. Diekwisch, D. Chen, Activation of beta-catenin signalling leads to temporomandibular joint defects, *Eur. Cell. Mater.* 28 (2014) 223–235.
- [6] M. Zhu, D. Tang, Q. Wu, S. Hao, M. Chen, C. Xie, R.N. Rosier, R.J. O'Keefe, M. Zuscik, D. Chen, Activation of beta-catenin signaling in articular chondrocytes leads to osteoarthritis-like phenotype in adult beta-catenin conditional activation mice, *J. Bone Miner. Res.* 24 (1) (2009) 12–21.
- [7] K. Lu, Q. Wang, H. Jiang, J. Li, Z. Yao, Y. Huang, J. Chen, Y. Zhang, G. Xiao, X. Hu, Z. Luo, L. Yang, L. Tong, D. Chen, Upregulation of beta-catenin signaling represents a single common pathway leading to the various phenotypes of spinal degeneration and pain, *Bone Res* 11 (1) (2023) 18.
- [8] Y. Zhou, T. Wang, J.L. Hamilton, D. Chen, Wnt/beta-catenin signaling in osteoarthritis and in other forms of arthritis, *Curr. Rheumatol. Rep.* 19 (9) (2017) 53.
- [9] K. Lu, F. Ma, D. Yi, H. Yu, L.P. Tong, D. Chen, Molecular signaling in temporomandibular joint osteoarthritis, *J Orthop Transl* 32 (2022) 21–27.
- [10] S.Y. Hwang, X.M. Deng, S. Byun, C. Lee, S.J. Lee, H. Suh, J.M. Zhang, Q.F. Kang, T. Zhang, K.D. Westover, A. Mandinova, S.W. Lee, Direct targeting of beta-catenin by a small molecule stimulates proteasomal degradation and suppresses oncogenic wnt/beta-catenin signaling, *Cell Rep.* 16 (1) (2016) 28–36.
- [11] M. Furtado, L. Chen, Z. Chen, A. Chen, W. Cui, Development of fish collagen in tissue regeneration and drug delivery, *Engineered Regeneration* 3 (3) (2022) 217–231.
- [12] X. Lin, L. Cai, X. Cao, Y. Zhao, Stimuli-responsive silk fibroin for on-demand drug delivery 2 (2) (2023) e20220019.
- [13] W. Zhou, X. Ma, J. Wang, X. Xu, O. Koivisto, J. Feng, T. Viitala, H. Zhang, Co-delivery CPT and PTX prodrug with a photo/thermo-responsive nanoplatfor for triple-negative breast cancer therapy 1 (1) (2022) e20220036.
- [14] Z.H. Sheng, D.H. Hu, M.B. Zheng, P.F. Zhao, H.L. Liu, D.Y. Gao, P. Gong, G.H. Gao, P.F. Zhang, Y.F. Ma, L.T. Cai, Smart human serum albumin-indocyanine green nanoparticles generated by programmed assembly for dual-modal imaging-guided cancer synergistic phototherapy, *ACS Nano* 8 (12) (2014) 12310–12322.
- [15] G.J. Deng, T. Zhu, L.H. Zhou, J.N. Zhang, S.P. Li, Z.H. Sun, J.Z. Lai, X.Q. Meng, W. J. Li, P.F. Zhang, Y.Y. Wu, T. Jiang, D.P. Ni, W.Q. Yan, M.B. Zheng, P. Gong, L. T. Cai, Bovine serum albumin-loaded nano-selenium/ICG nanoparticles for highly effective chemo-photothermal combination therapy, *RSC Adv.* 7 (49) (2017) 30717–30724.
- [16] K. Lu, Q. Wang, L. Hao, G. Wei, T. Wang, W.W. Lu, G. Xiao, L. Tong, X. Zhao, D. Chen, miR-204 ameliorates osteoarthritis pain by inhibiting SP1-LRP1 signaling and blocking neuro-cartilage interaction, *Bioact. Mater.* 26 (2023) 425–436.
- [17] S.S. Glasson, T.J. Blanchet, E.A. Morris, The surgical destabilization of the medial meniscus (DMM) model of osteoarthritis in the 129/SvEv mouse, *Osteoarthritis Cartilage* 15 (9) (2007) 1061–1069.
- [18] J. Li, Y. Wang, D. Chen, R. Liu-Bryan, Oral administration of berberine limits post-traumatic osteoarthritis development and associated pain via AMP-activated protein kinase (AMPK) in mice, *Osteoarthritis Cartilage* 30 (1) (2022) 160–171.
- [19] S. Zaki, M.M. Smith, C.B. Little, Pathology-pain relationships in different osteoarthritis animal model phenotypes: it matters what you measure, when you measure, and how you got there, *Osteoarthritis Cartilage* 29 (10) (2021) 1448–1461.
- [20] J. Li, B. Zhang, W. Liu, Metformin limits osteoarthritis development and progression through activation of AMPK signalling, vol 79, pg 635, 2020, *Ann. Rheum. Dis.* 79 (9) (2020).
- [21] S. Kamekura, K. Hoshi, T. Shimoaka, U. Chung, H. Chikuda, T. Yamada, M. Uchida, N. Ogata, A. Seichi, K. Nakamura, H. Kawaguchi, Osteoarthritis development in novel experimental mouse models induced by knee joint instability, *Osteoarthritis Cartilage* 13 (7) (2005) 632–641.
- [22] Y. Tamamura, T. Otani, N. Kanatani, E. Koyama, J. Kitagaki, T. Komori, Y. Yamada, F. Costantini, S. Wakasaka, M. Pacifici, M. Iwamoto, M. Enomoto-Iwamoto, Developmental regulation of Wnt/ β -catenin signals is required for growth plate assembly, cartilage integrity, and endochondral ossification, *J. Biol. Chem.* 280 (19) (2005) 19185–19195.
- [23] M. Zhu, D.Z. Tang, Q.Q. Wu, S.Y. Hao, M. Chen, C. Xie, R.N. Rosier, R.J. O'Keefe, M. Zuscik, D. Chen, Activation of β -catenin signaling in articular chondrocytes leads to osteoarthritis-like phenotype in adult β -catenin conditional activation mice, *J. Bone Miner. Res.* 24 (1) (2009) 12–21.
- [24] M.N. Wang, J. Shen, H.T. Jin, H.J. Im, J. Sandy, C. Chen, Recent progress in understanding molecular mechanisms of cartilage degeneration during osteoarthritis, *Skeletal Biology and Medicine II: Bone and Cartilage Homeostasis and Bone Disease* 1240 (2011) 61–69.
- [25] A. De Palma, G. Nalesso, WNT signalling in osteoarthritis and its pharmacological targeting, *Handb. Exp. Pharmacol.* 269 (2021) 337–356.
- [26] M.J. Alcaraz, J. Megias, I. Garcia-Arnandis, V. Clerigues, M.I. Guillen, New molecular targets for the treatment of osteoarthritis, *Biochem. Pharmacol.* 80 (1) (2010) 13–21.
- [27] J. Cheng, M. Li, R. Bai, The Wnt signaling cascade in the pathogenesis of osteoarthritis and related promising treatment strategies, *Front. Physiol.* 13 (2022) 954454.
- [28] X. Zhang, L. Wang, Y. Qu, Targeting the beta-catenin signaling for cancer therapy, *Pharmacol. Res.* 160 (2020) 104794.
- [29] N. Pecina-Slaus, S. Anicic, A. Bukovac, A. Kafka, Wnt signaling inhibitors and their promising role in tumor treatment, *Int. J. Mol. Sci.* 24 (7) (2023) 6733.
- [30] R. Jackstadt, M.C. Hodder, O.J. Sansom, WNT and β -catenin in cancer: genes and therapy, *Annu. Rev. Cell Biol.* 4 (2020) 177–196.
- [31] C. Lietman, B. Wu, S. Lechner, A. Shinar, M. Sehgal, E. Rossomacha, P. Datta, A. Sharma, R. Gandhi, M. Kapoor, P.P. Young, Inhibition of Wnt/ β -catenin signaling ameliorates osteoarthritis in a murine model of experimental osteoarthritis, *Jci Insight* 3 (3) (2018).
- [32] A. Held, A. Glas, L. Dietrich, M. Bollmann, K. Brandstädter, T.N. Grossmann, C. H. Lohmann, T. Pap, J. Bertrand, Targeting β -catenin dependent Wnt signaling via peptidomimetic inhibitors in murine chondrocytes and OA cartilage, *Osteoarthritis Cartilage* 26 (6) (2018) 818–823.
- [33] H. Song, K.H. Park, Regulation and function of SOX9 during cartilage development and regeneration, *Semin. Cancer Biol.* 67 (Pt 1) (2020) 12–23.
- [34] S.Y. Hwang, X.M. Deng, S. Byun, C. Lee, S.J. Lee, H. Suh, J.M. Zhang, Q.F. Kang, T. Zhang, K.D. Westover, A. Mandinova, S.W. Lee, Direct targeting of β -catenin by a small molecule stimulates proteasomal degradation and suppresses oncogenic wnt/ β -catenin signaling, *Cell Rep.* 16 (1) (2016) 28–36.
- [35] T. van der Wal, R. van Amerongen, Walking the tight wire between cell adhesion and WNT signalling: a balancing act for β -catenin, *Open Biol* 10 (12) (2020).
- [36] T. van der Wal, R. van Amerongen, Walking the tight wire between cell adhesion and WNT signalling: a balancing act for β -catenin, *Open Biol* 10 (12) (2020) 200267.
- [37] M. Hirose, A. Tachibana, T. Tanabe, Recombinant human serum albumin hydrogel as a novel drug delivery vehicle, *Mat Sci Eng C-Mater* 30 (5) (2010) 664–669.
- [38] F. Kratz, Albumin as a drug carrier: design of prodrugs, drug conjugates and nanoparticles, *J. Contr. Release* 132 (3) (2008) 171–183.
- [39] M. Fasano, S. Curry, E. Terreno, M. Galliano, G. Fanali, P. Narciso, S. Notari, P. Ascenzi, The extraordinary ligand binding properties of human serum albumin, *IUBMB Life* 57 (12) (2005) 787–796.
- [40] F. Lin, Y. Li, W. Cui, Injectable hydrogel microspheres in cartilage repair, *Biomedical Technology* 1 (2023) 18–29.
- [41] M. Shyngys, J. Ren, X. Liang, J. Miao, A. Blocki, S. Beyer, Metal-organic framework (MOF)-Based biomaterials for tissue engineering and regenerative medicine, *Front. Bioeng. Biotechnol.* 9 (2021) 603608.
- [42] S. Sebak, M. Mirzaei, M. Malhotra, A. Kulmarva, S. Prakash, Human serum albumin nanoparticles as an efficient noscapine drug delivery system for potential use in breast cancer: preparation and in vitro analysis, *Int. J. Nanomed.* 5 (2010) 525–532.
- [43] Z.K. Chen, L.L. Liu, R.J. Liang, Z.Y. Luo, H.M. He, Z.H. Wu, H. Tian, M.B. Zheng, Y. F. Ma, L.T. Cai, Bioinspired hybrid protein oxygen nanocarrier amplified photodynamic therapy for eliciting anti-tumor immunity and abscopal effect, *ACS Nano* 12 (8) (2018) 8633–8645.
- [44] Y.M. Luo, Z. Chen, M.J. Sun, B.H. Li, F. Pan, A.Q. Ma, J.H. Liao, T. Yin, X.F. Tang, G.J. Huang, B.Z. Zhang, H. Pan, M.B. Zheng, L.T. Cai, IL-12 nanochaperone-engineered CAR T cell for robust tumor-immunotherapy, *Biomaterials* 281 (2022) 121341.
- [45] L. Xiao, C. Liu, B. Wang, W. Fei, Y. Mu, L. Xu, Y. Li, Targeting discoidin domain receptor 2 for the development of disease-modifying osteoarthritis drugs, *Cartilage* 13 (2 suppl) (2021) 1285S–1291S.
- [46] J. Wang, H. Lu, X. Liu, Y. Deng, T. Sun, F. Li, S. Ji, X. Nie, L. Yao, Functional analysis of discoidin domain receptor 2 in synovial fibroblasts in rheumatoid arthritis, *J. Autoimmun.* 19 (3) (2002) 161–168.
- [47] W. Zhao, C. Zhang, M. Shi, J. Zhang, M. Li, X.C. Xue, Z. Zhang, Z. Shu, J.Y. Zhu, N. Mu, W.N. Li, Q. Hao, Z.J. Wang, L. Gong, W. Zhang, Y.Q. Zhang, The discoidin domain receptor 2/annexin A2/matrix metalloproteinase 13 loop promotes joint

- destruction in arthritis through promoting migration and invasion of fibroblast-like synoviocytes, *Arthritis Rheumatol.* 66 (9) (2014) 2355–2367.
- [48] A. Kumar, M.D. Choudhury, P. Ghosh, P. Palit, Discoidin domain receptor 2: an emerging pharmacological drug target for prospective therapy against osteoarthritis, *Pharmacol. Rep.* 71 (3) (2019) 399–408.
- [49] L.B. Manning, Y.F. Li, N.S. Chickmagalur, X.L. Li, L. Xu, Discoidin domain receptor 2 as a potential therapeutic target for development of disease-modifying osteoarthritis drugs, *Am. J. Pathol.* 186 (11) (2016) 3000–3010.